JOM, Vol. 69, No. 3, 2017
DOI: 10.1007/s11837-016-2231-4

Optimization of Binder Jetting Using Taguchi Method

SANJAY SHRESTHA[1] and GUHA MANOGHARAN[2,3]

1.—Department of Mechanical and Industrial Engineering, Youngstown State University, Youngstown, OH 44555, USA. 2.—Department of Mechanical and Nuclear Engineering, The Pennsylvania State University, University Park, PA 16801, USA. 3.—e-mail: gum53@psu.edu

Among several additive manufacturing (AM) methods, binder-jetting has undergone a recent advancement in its ability to process metal powders through selective deposition of binders on a powder bed followed by curing, sintering, and infiltration. This study analyzes the impact of various process parameters in binder jetting on mechanical properties of sintered AM metal parts. The Taguchi optimization method has been employed to determine the optimum AM parameters to improve transverse rupture strength (TRS), specifically: binder saturation, layer thickness, roll speed, and feed-to-powder ratio. The effects of the selected process parameters on the TRS performance of sintered SS 316L samples are studied with the American Society of Testing Materials (ASTM) standard test method. It was found that binder saturation and feed-to-powder ratio were the most critical parameters, which reflects the strong influence of binder powder interaction and density of powder bed on resulting mechanical properties. This article serves as an aid in understanding the optimum process parameters for binder jetting of SS 316L.

INTRODUCTION

Additive manufacturing (AM) is defined as "[t]he process of joining materials to make objects from three dimensional (3D) model data, usually layer upon layer, as opposed to subtractive manufacturing methodologies."[1] Additive manufacturing has a wide range of applications, most notably, automotive, aerospace, biomedical, and energy generation.[2] The American Society of Testing Materials (ASTM-F42) recognizes seven categories of AM processes based on principles of operations: direct energy deposition, sheet lamination, powder bed fusion, material extrusion, binder jetting, material jetting, and vat photo-polymerization.[1]

Binder jetting is defined as "an additive manufacturing process in which a liquid bonding agent is selectively deposited to join powder materials."[1] A layer of powder is spread across the build platform and binders are selectively deposited based on computer-aided drafting (CAD) model information in each layer. This process is repeated until the final geometry is achieved. In the case of metal binder-jetting systems, the entire powder bed is "cured" to burn off the binder and to retrieve the final part. Subsequently, the part is sintered to create metallurgical bonding and often infiltrated with a material of lower melting point to achieve higher density.[3,4] This AM process has found applications in sand-printing of cores and molds for foundry industries.[5] Unused powder is recycled for subsequent builds similar to other AM processes. The parts produced through this method have varied applications based on material (e.g., plaster, metal, sand, and polymers) and binder (e.g. water-based, organic, and multiple color), and based on specific applications, secondary infiltration of elastomers, wax, and metals are required.[6]

Binder jetting is one of the more flexible technologies because the process is independent of power source or other temperature-related constraint within the AM build envelope. Hence, a wide variety of materials can be processed through binder jetting (metal, sand, glass, ceramics, wood, cornstarch, etc.) without the need for support structures found in other AM methods.[3] When compared with powder-bed fusion (PBF) methods (e.g. Laser-PBF and electron beam melting), there are limited studies on optimization and parameter development in binder jetting. Process parameter optimization and resulting mechanical properties from AM production are critical for end-applications. A recent optimization study focused on dimensional accuracy (shrinkage) and surface finish

(Published online January 3, 2017)

in binder-jetting AM of 420 Stainless Steel (SS).[7] It was identified that layer thickness and binder saturation that affected surface finish and drying time had the most influence on part shrinkage.[7] Another recent study focused on the elastic modulus of 316 SS lattice structures produced using binder jetting and found that mechanical properties were much lower than comparable AM methods using default layer thickness, binder saturation, heater power ratio, and drying time.[8]

A fractional factorial experimental study on compressive properties of porous bio-composite (316L SS and Calcium Phosphate Tribasic) as a function of layer thickness, roller speed, sintering time, and sintering temperature revealed an inconclusive effect on those parameters as a result of the limited amount of data from the study.[9] M. Vaezi and C.K. Chua studied the effect of layer thickness and binder saturation on mechanical strength and surface quality of ZP102® plaster-based powder and found that at the uniform layer thickness, an increase in binder saturation resulted in increased tensile and flexural strength but in poorer dimensional accuracy. On the other hand, under uniform binder saturation, larger layer thickness resulted in decreased tensile strength and in increased flexural strength but improved the surface quality.[10] Another study focused on energy and material consumption of binder-jetting and validated a unit-process level model to provide life-cycle inventory data for further life-cycle analysis of the binder-jetting AM process.[11] There have been several optimization studies in binder-jetting of plaster,[12,13] gypsum-based,[14] and polymer components,[15] and it was consistently found that layer thickness, binder saturation, and location of the part in the build envelope were critical variables.[16,17]

It should be noted that in the case of metal AM binder-jetting, the metal powder is typically atomized (air or inert gas) and there is an additional need to understand its influence on the resulting mechanical properties. Nevertheless, with the exceptions of few studies,[7,8] there has been limited work on the optimization of binder jetting in metal AM. It is critical to evaluate the relationship between process parameters akin to prior nonmetal binder-jetting studies but also to include packing density (roll speed and feed-to-powder ratio, i.e., thickness of feed layer/layer thickness). This study applies the Taguchi optimization method to study the relationship between print parameters and transverse rupture strength of sintered 316L stainless steel.

Various methods have been employed to optimize manufacturing processes. These include genetic algorithm, geometric programming, geometric plus linear programming, scatter search technique, and response surface methodology. The Taguchi method, which was proposed by Japanese engineer Genichi Taguchi, is an optimization approach that comprises experimental design and statistical analysis to improve the product quality by integrating quality control at the design stages. The basic goal is to represent the effect or benefit of the process as

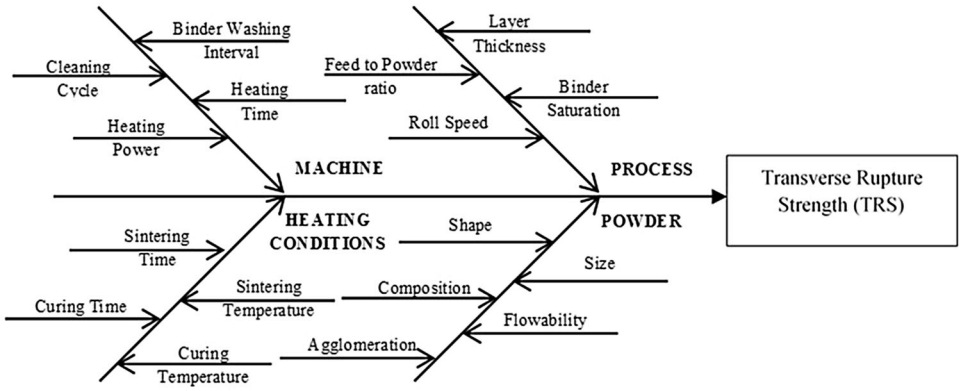

Fig. 1. Fishbone diagram for binder-jetting process.

Table I. Printing parameters with their ranges and values at three levels

Parameter design	Printing parameters	Range	Level 1	Level 2	Level 3
A	Saturation	35–100%	35	70	100
B	Layer Thickness	80–120 μm	80	100	120
C	Roll Speed	6–14 mm/s	6	10	14
D	Feed-to-Powder Ratio	1–3	1	2	3

a function of certain design variables with an overall objective to maximize or minimize the value of the function within the manufacturing process. This approach employs a quality measure called the "signal-to-noise ratio" to choose control levels that could best cope with changes in operating and environmental conditions, or noise. Although this method has been employed in the field of marketing, business, and biotechnology, it is particularly valuable in the "off-line" analysis of manufacturing processes.

For instance, surface finish and hole diameter accuracy in dry drilling of Al 2024 alloy was analyzed for varying cutting speed, feed rate, depth, and tool material.[18] Other studies have employed this method in optimizing manufacturing parameters in brake lining,[19] plastic injection molding,[20] die casting,[21] selective laser sintering,[22] fused deposition modeling,[14] and evaluation of different AM processes to fabricate injection molds.[23] The major advantage of using the Taguchi method is its straightforward approach that enables the analysis of multiple parameters without the need for a large number of experimentation. Through an orthogonal array-based design of experiments, key parameters that have the most effect on performance characteristics value are identified. This helps in identifying critical variables for a more detailed analysis, and the parameters that have little effect can be ignored in subsequent studies. Nevertheless, a disadvantage of this approach is that the results obtained are only relative to the initial selection of process parameters and do not indicate the parameter across all process variables, which might have the highest effect on the performance.

MATERIALS AND EXPERIMENTAL METHODS

The motivation for this study is to understand the effects of print parameters on the mechanical strength of sintered metal AM parts using the Taguchi method. The fish-bone diagram (Ishikawa diagram) shown in Fig. 1 provides an overview of process parameters in binder jetting that could affect the transverse rupture strength (TRS) of the samples. It should be noted that more than 20 parameters are involved in binder jetting that can be classified as process-related parameters (e.g., binder saturation, roll speed, layer thickness, feed-to-powder ratio), machine-based (e.g., heating time, heating power, binder washing interval, and cleaning cycle), post-AM-related parameters (e.g., sintering time, curing time, curing temperature, and sintering temperature) and powder based (e.g., size, shape, composition, flowability, and agglomeration).

Based on the findings from prior studies[16,17] and on improved flowability of atomized metal powders, the following parameters are studied: Saturation Level (A), Layer Thickness (B), Roll Speed (C), and Feed-to-Powder Ratio (D) as shown in Table I. TRS is a commonly used measure of mechanical strength in powder-metallurgy (akin to sintered binder-jet AM metal parts without infiltration). The rationale behind selecting these parameters is that (I) saturation level (percentage of volume occupied by binder in each layer) and layer thickness (minimum thickness of the material layer) will influence binder–powder interaction as identified from prior work in binder-jetting of nonmetal parts[7,8,15–17] and (II) roll speed (speed of the powder spread across the printing bed) and feed-to-powder ratio (thickness of feed layer/layer thickness) will influence the packing density of each layer because the atomized metal powder exhibits superior flowability.[24] With growing interest in binder-jet processing of nonatomized feedstock material such as metal oxide,[25] porcelain ceramic,[26] sand,[27] and silicon-nitride,[28] it is important to evaluate the impact of packing density on the resulting mechanical property.

Standard ASTM B528-99 specimen of nominal dimensions 31.7 mm × 12.7 mm × 6.35 mm were printed in X-1 Lab Ex-One using 316L Stainless Steel powder supplied by ExOne. The samples were cured at 190°C for 4 h. The cured sampled were sintered in vacuum with the following temperature-time cycle recommended by Ex-One: (I) 5°C/min ramp up to 700°C, 1-h dwell; (II) 5°C/min ramp up to 1120°C, 2 h dwell; (III) cool down at 5°C/min to 850°C, 1 min; and (IV) cool down at 5°C/min to room temperature. The orthogonal array L27 corresponding to this study is presented in the online supplementary material. The orientation of the specimen during its build plays an important role as it affects the final mechanical properties of the specimen. Hence, for this study, all the samples were built along the direction that is perpendicular to the direction of loading. Based on ASTM B528-99, a 76.2-mm hardened rod was used for testing at a loading rate of 2.5 mm/min until complete rupture occurred. The transverse rupture strength of the sample is given by:[29]

$$\mathrm{TRS} = (3PL)/(2t^2w) \tag{1}$$

where P = force required to rupture the specimen (N), L = length of the specimen span relative to fixture (mm), w = width of the specimen, in. (mm), t = thickness of specimen, in. (mm).

After sintering, a digital caliper was used to record the sample dimensions (five measurements per sample). Instron 5500R with a maximum load rating of 100 kN was used to conduct testing, and Instron Bluehill 2 was used to record the load data. As the aim of this study was to focus on powder–binder interaction and packing density, the effects of A, B, C, D, and first-order and second-order interaction between $A \times B$, $A \times C$, and $C \times D$ are considered. Because four factors at three levels each are studied, orthogonal array L_{27} (3^13) with four samples per run is selected because full interactions could be conducted in future studies. Along with

Table II. TRS and S/N ratios against L_{27} run

Run	Trial 1	Trial 2	Trial 3	Trial 4	TRS (MPa)	S/N ratio
1	33.16	36.38	56.83	40.93	41.82	31.92
2	52.94	36.81	38.22	62.35	47.58	32.93
3	38.88	55.08	45.80	63.40	50.79	33.67
4	54.19	69.43	60.82	51.76	59.05	35.26
5	49.76	63.19	67.21	67.49	61.91	35.63
6	45.68	33.10	57.18	74.32	52.57	33.28
7	52.61	90.65	78.92	95.55	79.43	37.25
8	30.17	41.00	41.87	41.02	38.52	31.46
9	34.26	39.97	41.10	44.55	39.97	31.88
10	76.28	77.50	65.66	92.30	77.93	37.65
11	67.42	71.50	96.87	58.80	73.65	36.93
12	60.30	52.65	76.57	58.17	61.92	35.60
13	94.44	86.28	112.59	67.11	90.10	38.64
14	65.76	54.86	58.15	73.81	63.14	35.84
15	81.88	69.75	58.34	79.38	72.34	36.95
16	56.26	62.00	99.76	72.90	72.73	36.65
17	64.90	76.29	87.51	70.60	74.82	37.33
18	44.10	65.31	83.34	115.78	77.13	36.17
19	64.32	55.35	71.57	85.01	69.06	36.47
20	84.75	49.89	50.54	53.13	59.58	34.93
21	92.36	79.84	61.12	67.26	75.14	37.20
22	80.75	55.76	32.55	64.01	58.27	33.81
23	87.07	69.23	105.59	53.26	78.79	37.08
24	107.26	65.43	78.10	82.05	83.21	38.01
25	83.87	53.61	75.81	74.03	71.83	36.74
26	71.30	64.72	92.26	61.39	72.42	36.89
27	53.13	80.08	52.86	53.58	59.91	35.17

Table III. Average values of S/N ratios at the different levels and their main effects

Parameters	S.N. Level 1	S.N. Level 2	S.N. Level 3	S.N. Level 2–Level 1	S.N. Level 3–Level 2
A	33.78	37.21	36.68	3.43	−0.53
B	35.26	36.37	35.30	1.11	−1.08
C	36.13	35.35	35.40	−0.78	0.05
D	34.54	35.70	36.92	1.16	1.22

mean response, the signal-to-noise ratio (S/N) is calculated to analyze the variation in response variable (i.e., TRS). The TRS is a "larger-is-better" type of quality characteristics, and the corresponding S/N ratio is given by:

$$\frac{\mathrm{S}}{\mathrm{N}}\text{ratio (dB)} = -10\log\left[\frac{1}{n}\sum_{i=1}^{n}\left(\frac{1}{\mathrm{TRS}_i^2}\right)\right] \qquad (2)$$

where TRS_i is the response variable for n repetition for each treatment condition.

RESULTS AND DISCUSSION

The average values of TRS and S/N ratios at all three levels for each parameter are shown in Tables II and III, and they are presented in Fig. 2. Table III also presents the main effects of the parameters (A, B, C, and D) when variable level is increased.

It is evident from Fig. 2 that the second level for parameters A, B (saturation level of 70% and layer thickness of 100 μm), first level for parameter C (roll speed of 6 mm/s), and third level for parameter D (feed-to-powder ratio of 3) provided the largest TRS value and S/N ratio.

Representative SEM images of fracture surfaces shown in Fig. 3 highlight lower contact sites between particles for sample with the lowest TRS value when compared with the fracture surface of the sample with the highest TRS value. ANOVA analysis at 95% CI is performed to study the significance of the parameters. ANOVA analysis

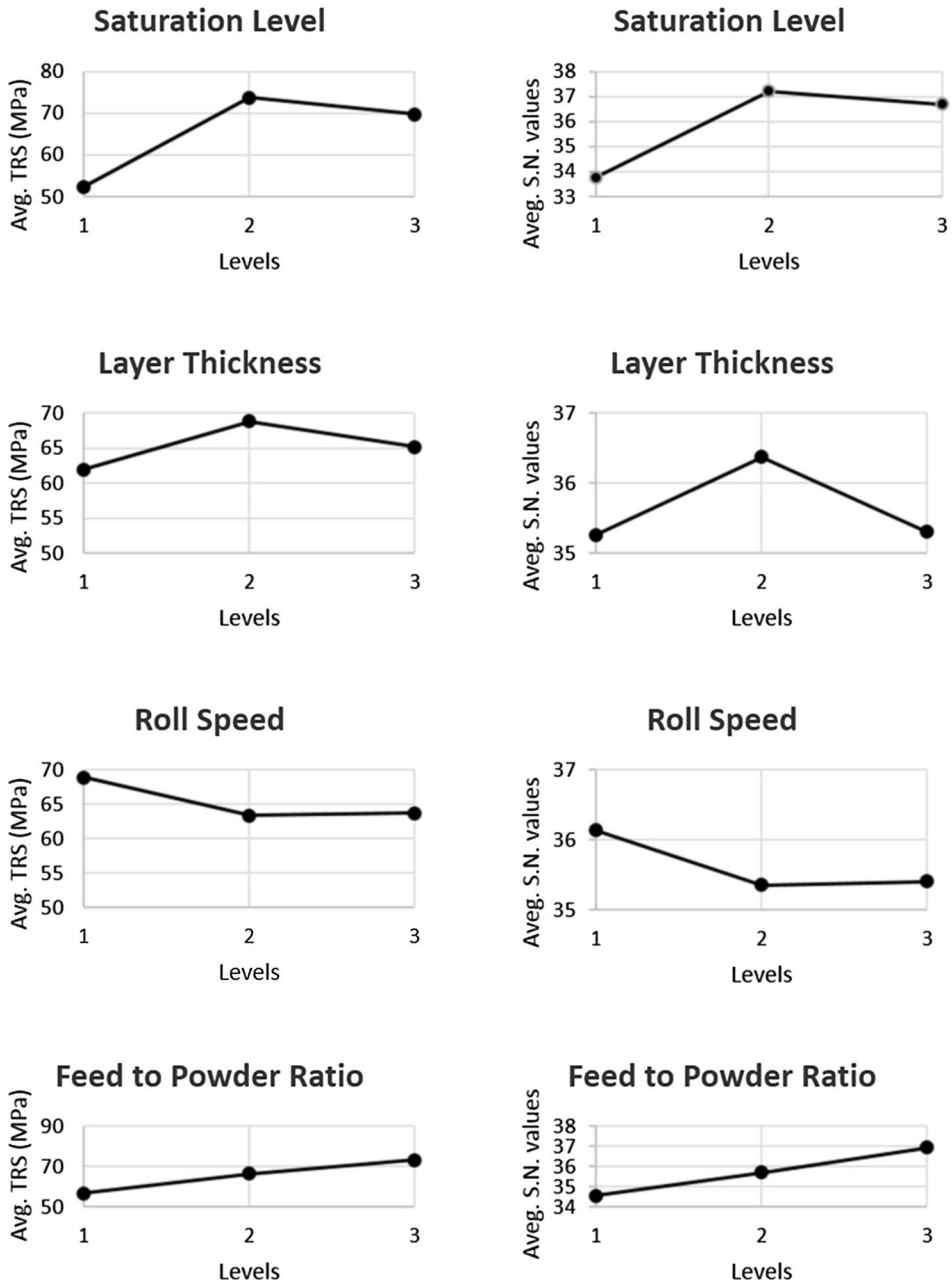

Fig. 2. Average values of TRS and S/N ratio for each parameter at levels 1–3.

shown in Table IV identifies that saturation level (A) and feed-to-powder ratio (D) are the critical parameters that significantly affect the mean TRS.

The long-range mean estimation of TRS is achieved by using the estimation model of Taguchi based on the average values of levels of factors and their equivalent β-factors, which is given by the equation:[30]

$$\mu = M\text{ß}(M) + (A2 - M)\text{ß}(A) + (B2 - M)\text{ß}(B) + (C1 - M)\text{ß}(C) + (D3 - M)\text{ß}(D) \quad (3)$$

where M is the overall average of the trials; ß(A), ß(B), ß(C), and ß(D), are the ß-factors of A–D, respectively; and is defined by:

$$\text{ß}(P) = 1 - \frac{1}{F_P} \quad (4)$$

where F_P is the F-ratio of the factor P.

$A2$, $B2$, $C1$, and $D3$ are the optimal levels of the control parameters. The ß (M) is the overall ß-factor, which is defined by:

$$\text{ß}(M) = 1 - \frac{V_e}{T} \quad (5)$$

where V_e is the variance resulting from the error and T is the sum of square of trails. Using Eq. 4, the long-range mean performance for estimated transverse rupture strength is calculated as

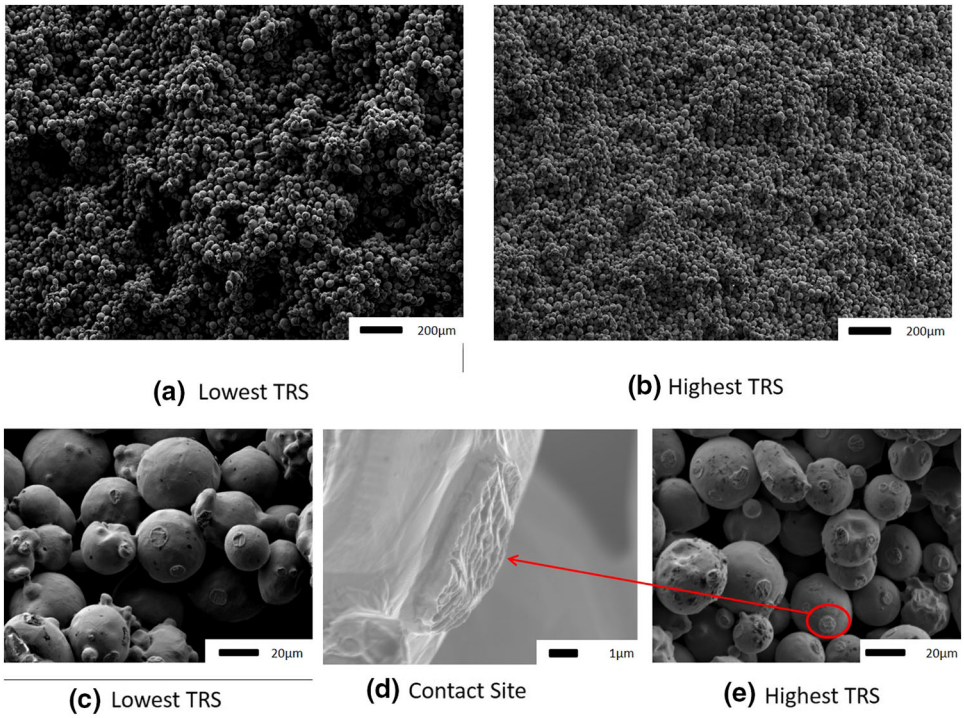

Fig. 3. Macro-scale SEM Images (100-μm scale) and micro-scale SEM Images (10 μm) of the sample with lowest (a, c), highest (b, e) TRS values and contact site (d).

Table IV. ANOVA average TRS values

Source	Sum Sq.	*df*	Mean Sq.	*F*	Prob > *F*
A	9288	2	4643.98	20.78	0.0000
B	852.3	2	426.15	1.91	0.1548
A × B	8.4	2	4.18	0.02	0.9815
$(A \times B)^2$	238.1	2	119.06	0.53	0.589
C	699.6	2	349.78	1.56	0.215
(A × C)	764.9	2	382.47	1.71	0.1867
$(A \times C)^2$	583.6	2	291.78	1.31	0.2763
D	5011	2	2505.5	11.21	0.0000
C × D	240	2	120.02	0.54	0.5865
$(C \times D)^2$	446.5	2	223.27	1.	0.3725
Error	194,474	87	223.53		
Total	37,579.7	107			

μ = 83.34 MPa. Similarly, the confidence interval (CI) for the estimation can be computed using the following equation:[30]

$$\text{C.I.} = \pm\sqrt{(F(1, \alpha, d.f_e) \times V_e/N_e)} \quad (6)$$

where F (1, α, $d.f_e$) is the required F-ratio for α risk, DOF of error $d.f._e$, V_e is the pooled error variance, and N_e is the effective sample size given by:

$$N_e = N/\left[1 + \sum_P (u_P ß(P))\right] \quad (7)$$

where N is the total number of trials, u_P is the DOF of factor, and ß(P) is the ß-factor if factor P.

For a confidence interval of 95% for the TRS; F-ratio (1, 5%, 87) = 3.96 and V_e = 223.53, the effective sample size is determined to be 16.86. Hence, the CI is computed as 7.25, and subsequently, the confidence interval of the predicted optimum is given as 76.09 MPa < μ < 90.59 MPa. The identified critical variables are consistent with prior optimization studies on the binder-jetting AM process.[7,8,17]

CONCLUSION

This study applied an optimization method in the Taguchi approach to a lesser studied binder-jetting AM of metal parts. Four variables (binder saturation, layer thickness, roll speed, and feed-to-powder ratio) were analyzed to maximize the transverse rupture strength of 316L SS parts. The conclusions from the study are summarized as follows:

1. It was found that saturation level and feed-to-powder ratio were the critical parameters. A higher percentage of volume for binder and densification of powder layer at higher ratio of feed-to-layer thickness ratio improves both powder–binder interaction and densification.
2. The optimal levels for each printing parameters for the optimum transverse rupture strength are as follows:

Binder Saturation (%)	70
Layer Thickness (μm)	100
Roll speed (mm/s)	6
Feed to powder ratio	3

3. The estimated long-range mean for the transverse rupture strength was calculated to be 83.34 MPa. The predicted range for the optimum transverse rupture strength was 76.09 MPa < TRS < 90.59 MPa. With the optimal parameters, the TRS value changed from an average of 65.32 MPa to 90.59 MPa with an increase of 38.69%. Future studies will incorporate sintering cycles as a variable (time-temperature profile) to decrease porosity and extend this work with other alloy systems.

ELECTRONIC SUPPLEMENTARY MATERIAL

The online version of this article (doi:10.1007/s11837-016-2231-4) contains supplementary material, which is available to authorized users.

REFERENCES

1. ASTM F2792-12a, *Standard Terminology for Additive Manufacturing Technologies* (2011), pp. 1–3.
2. T.T. Wohlers, Wohlers Report 2015. *Wohlers Associates* 2015, 23 (2015).
3. A.M. Knudson, I.A. Popernack, and A. Schuler, *Int. J. Metall. Cast.* 10, 111 (2016).
4. H. Ludwig, and T. Joel, *Wear Properties of 3D Printed Stainless Steel-Bronze Composite* (Minnesota State University—Mankato, Undergraduate Research Symposium, 2015), http://cornerstone.lib.mnsu.edu/urs/2015/poster_session_A/2/. Accessed 20 October 2016.
5. D. Snelling, Q. Li, N. Meisel, C.B. Williams, R.C. Batra, and A.P. Druschitz, *Adv. Eng. Mater.* 17, 923 (2015).
6. I. Gibson, D. Rosen, and B. Stucker, *Additive Manufacturing Technologies: 3D Printing, Rapid Prototyping, and Direct Digital Manufacturing*, 2nd ed. (New York: Springer, 2015), pp. 205–218.
7. H. Chen and Y.F. Zhao, *Rapid Prototyp. J.* 22, 527 (2016).
8. Y. Tang, Y. Zhou, T. Hoff, M. Garon, and Y.F. Zhao, *Mater. Sci. Technol.* 32, 648 (2016).
9. D.S.D. Uduwage, *Binder Jet Additive Manufacturing of Stainless Steel-Hydroxyapatite Bio-composite* (Minnesota State University—Mankato, Masters Thesis, 2015), http://cornerstone.lib.mnsu.edu/etds/432/. Accessed 15 September 2016.
10. M. Vaezi and C.K. Chua, *Int. J. Adv. Manuf. Technol.* 53, 275 (2010).
11. S. Meteyer, X. Xu, N. Perry, and Y.F. Zhao, *Proc. CIRP.* 15, 19 (2014).
12. A.W. Yao and Y.C. Tseng, *Rapid Prototyp. J.* 8, 180 (2002).
13. J. Suwanprateeb, F. Thammarakcharoen, K. Wasoontararat, and W. Suvannapruk, *Rapid Prototyp. J.* 18, 490 (2012).
14. T.J. Hsu and H.W. Lai, *J. Chin. Inst. Eng.* 33, 121 (2010).
15. J. Suwanprateeb, *Polym. Int.* 55, 57 (2006).
16. M. Chhabra and R. Singh, *Rapid Prototyp. J.* 18, 458 (2012).
17. S.J. Li and S. Cao, *Adv. Mater. Res.* 399, 1639 (2012).
18. M. Kurt, E. Bagci, and Y. Kaynak, *Int. J. Adv. Manuf. Technol.* 40, 458 (2009).
19. S.J. Kim, K.S. Kim, and H. Jang, *J. Mater. Process. Technol.* 136, 202 (2003).
20. H. Oktem, E. Tuncay, and I. Uzman, *Mater. Des.* 28, 1271 (2007).
21. G.P. Syrcos, *J. Mater. Process. Technol.* 135, 68 (2003).
22. K.S. Lakshmi and G. Arumaikkannu, *Adv. Mater. Res.* 845, 862 (2014).
23. I. Flores, E. Coatanea, M. Salmi, and J. Tuomi, *Robust Design Principles to Evaluate Additive Manufacturing Capabilities* (1st International Symposium on Robust Design, 2014), http://proceedings.dtu.dk/fedora/repository/dtu:2156/OBJ/S07_OralSession2_Flores.pdf. Accessed 17 September 2016.
24. J. Clayton, *Met. Powder Rep.* 69, 14 (2014).
25. G. Manogharan, M. Kioko, and C. Linkous, *J. Met. Mater. Miner.* 67, 660 (2015).
26. H. Miyanaji, S. Zhang, A. Lassell, A. Zandinejad, and L. Yang, *J. Met. Mater. Miner.* 68, 831 (2016).
27. E.S. Almaghariz, B.P. Conner, L. Lenner, R. Gullapalli, G.P. Manogharan, B. Lamoncha, and M. Fang, *Int. J. Metalcast.* 10, 240 (2016).
28. L. Rabinskiy, A. Ripetsky, S. Sitnikov, Y. Solyaev, and R. Kahramanov, *IOP Mater. Sci. Eng.* 140, 012023 (2016).
29. ASTM B 528-99, *Standard Test Method for Transverse Rupture Strength of Metal Powder Specimens* (2000), pp. 1–4.
30. R.K. Roy, *A Primer on the Taguchi Method*, 2nd ed. (Dearbon, MI: Society of Manufacturing Engineers, 2010).